Published as: *Nature*. 2008 August 21; 454(7207): 1009–1013.

Structural Mechanism of WASP Activation by the Enterohaemorrhagic *E. coli* Effector $EspF_U$

Hui-Chun Cheng[1], **Brian M. Skehan**[2], **Kenneth G. Campellone**[2], **John M. Leong**[2], and **Michael K. Rosen**[1,*]

[1]Department of Biochemistry and Howard Hughes Medical Institute, UT Southwestern Medical Center, Dallas, TX 75390

[2]Department of Molecular Genetics and Microbiology, University of Massachusetts Medical School, Worcester, MA 01655

Abstract

During infection enterohaemorrhagic *Escherichia coli* (EHEC) usurp the actin cytoskeleton of eukaryotic cells by injecting the $EspF_U$ protein into the host cytoplasm[1, 2]. $EspF_U$ controls actin by activating members of the Wiskott-Aldrich Syndrome Protein (WASP) family[1–5]. Here we show that $EspF_U$ binds the autoinhibitory GTPase binding domain (GBD) in WASP proteins and displaces it from the activity-bearing VCA domain. This interaction potently activates WASP and N-WASP *in vitro* and induces localized actin assembly in cells. In the solution structure of the GBD-$EspF_U$ complex, $EspF_U$ forms an amphipathic helix that binds the GBD, mimicking interactions of the VCA in autoinhibited WASP. Thus, $EspF_U$ activates by competing directly for the VCA binding site on the GBD. This mechanism is distinct from that used by the eukaryotic activators Cdc42 and SH2 domains, which globally destabilize the GBD fold to release the VCA[6–8]. Such diversity of mechanism in WASP proteins is distinct from other multi-modular systems, and may result from the intrinsically unstructured nature of the isolated GBD and VCA elements. The structural incompatibility of the GBD complexes with $EspF_U$ and Cdc42/SH2, plus high affinity $EspF_U$ binding, enable EHEC to potently hijack the eukaryotic cytoskeletal machinery.

Pathogenic bacteria often target the host actin cytoskeleton during infection to assist entry, cell-to-cell spreading, and intimate attachment to host membranes[9–13]. EHEC (serotype O157:H7) is a food-born human pathogen that causes severe diarrhea and hemolytic uremic syndrome[14]. During infection, EHEC binds eukaryotic host intestinal epithelial cells and secretes Tir (Translocated Intimin Receptor) and $EspF_U$ (also known as TccP), into the host cell[1, 2]. The secreted Tir localizes in the host plasma membrane, and upon clustering by binding to the bacterial outer surface protein intimin, recruits $EspF_U$ via its C-terminal cytoplasmic domain[3]. $EspF_U$ in turn hijacks members of the Wiskott-Aldrich Syndrome Protein (WASP) family, which locally stimulate the actin nucleation factor, Arp2/3 complex[1–5]. Together, these interactions induce the formation of an actin-rich membrane protrusion beneath the site of EHEC attachment, termed an actin pedestal[1, 2, 15].

WASP proteins activate Arp2/3 complex through a C-terminal VCA domain[16]. In free WASP, this activity is blocked through intramolecular interactions with a central GTPase binding domain (GBD). Structural and biochemical studies have shown that the GBD sequesters an

*Corresponding Author: Michael K. Rosen, Telephone: 214-645-6361, Fax: 214-645-6353, Email: E-mail: Michael.Rosen@utsouthwestern.edu.

Accession Number. Atomic coordinates of the 20 final lowest energy conformers have been deposited in the Protein Data Bank under accession code 2K42.

amphipathic helix in the C region of the VCA that is necessary for activation of Arp2/3 complex, resulting in autoinhibition[7, 17, 18]. WASP can be allosterically activated by a number of intracellular ligands, including Cdc42 and (for phosphorylated WASP) SH2 domains[8, 19]. These ligands bind to WASP and N-WASP in a manner that is structurally incompatible with the autoinhibited fold of the GBD. Thus, they activate by globally destabilizing the GBD, consequently releasing the VCA[6, 8, 20, 21].

$EspF_U$ is composed of an N-terminal signal sequence necessary for translocation into the eukaryotic host, followed by 2–7 nearly identical 47 residue repeats (Fig. 1A)[22]. Each full repeat consists of an N-terminal 27 residue hydrophobic segment and a C-terminal 20 residue proline-rich segment. Previous studies showed that $EspF_U$ can bind the N-WASP GBD and activate N-WASP toward Arp2/3 complex in actin assembly assays *in vitro*[1, 2, 4]. A similar sequence is found in the related bacterial effector EspF, which also can activate N-WASP (Fig. S1)[23].

To understand $EspF_U$-mediated activation, we examined fragments containing the full 47-residue fifth repeat (R47, Fig. 1, Fig. S1) and an N-terminal 33-residue fragment lacking most of the proline-rich sequence (R33). In Arp2/3-mediated pyrene-actin assembly assays, R47 and R33 significantly and similarly enhanced the activities of autoinhibited N-WASP and WASP proteins ($N\text{-}WASP_C$, and GBD-VCA, respectively; Fig. 1B, Fig. S2). Titration of R47 into N-WASPC produced a monotonic increase in actin assembly rate (Fig. 1C and Fig. S3), which reached a plateau value similar to that of the NWASP VCA. Thus, the endpoint of the titration produces a state which biochemically resembles free N-WASP VCA. Fitting the data to a single-site binding isotherm yields a K_{Act} of 24 nM, approximating the K_D of R47 for $N\text{-}WASP_C$, 35 nM (Fig. S4). $EspF_U$ binds N-WASP > 100-fold more strongly than does Cdc42[21], resulting in much greater potency in actin assembly assays (Fig. 1C). This much higher affinity should enable $EspF_U$ to hijack N-WASP away from its endogenous regulators *in vivo*[21].

Cdc42 and SH2 domains activate WASP by physically displacing the VCA from the GBD[7, 8]. $EspF_U$ R33 disrupts GBD-VCA interactions similarly (Fig. S5), indicating that it also binds the GBD in a manner that is incompatible with the autoinhibitory interactions. The combined data show that $EspF_U$ R33 is functionally equivalent to Cdc42 and SH2 domains: all three ligands activate WASP/N-WASP by releasing the VCA from the GBD.

The WASP GBD is largely unstructured on its own, but folds to a well-defined conformation upon binding VCA[7]. $^1H/^{15}N$ and $^1H/^{13}C$ amide and methyl TROSY NMR spectra showed that $EspF_U$ R33 or a five-repeat fragment, R_5, also induced folding of the GBD (Fig. S6). Reciprocally, the GBD induces folding of the unstructured R33 (Fig. S6B, Fig. S7). Titrations of R33 and R_5 into GBD saturated at 1:1 and 0.2:1 $EspF_U$:GBD stoichiometry, respectively, showing that each repeat can bind N-WASP. The endpoint spectra are strikingly similar, indicating that the GBD folds to the same structure on each repeat, and that the molecular nature of allosteric activation can be understood through analysis of the R33 complex.

We determined the solution structure of the WASP GBD in complex with $EspF_U$ R33 using NMR spectroscopy (Fig. 2, Fig. S8; Table S1). The complex can be considered in three stacked structural layers[7]. The first layer is composed of a short N-terminal i+4 β hairpin (β1, 252–253; β2, 257–258) and α1 helix (265–274) from the GBD. The second layer lies behind the first and consists of GBD helices α2–α4 (α2, 278–281; α3, 284–296; α4, 300–306), which have a roughly planar C-shaped arrangement. The third layer is an amphipathic α5 helix (3–14) and an extended arm (16–20) from $EspF_U$. These elements contact the back of the GBD and are roughly antiparallel to α3 and α2, respectively (Fig. 2A, structural details in Fig. S9). WASP residues 242–249 and $EspF_U$ residues 21–33 appear to be largely disordered in solution, based

on the absence of long range ^{1}H-^{1}H NOEs and low heteronuclear {^{1}H}-^{15}N NOEs (Fig. S10). The $EspF_U$ relative, EspF, is expected to bind the GBD through an analogous amphipathic α5 helix, but may not use an extended arm, as these C-terminal residues are not conserved (Fig. S1).

To better understand the physical basis of $EspF_U$ activity, we examined a series of single repeat mutants based on the structure. First, we fused these proteins C-terminally to the WASP GBD through a short linker. Since the GBD and R33 are only folded when bound to each other, the thermodynamic stability of the fusions reports on the relative strengths of interaction between the two elements. We mutated three conserved hydrophobic residues, V4, L8 and L12, which lie at the center of the interface between α5 and the GBD (Fig. S9). The L12A ($R33^{VL*}$) and V4A/L8A ($R33^{**L}$) mutants have substantially reduced stability relative to wild type in the GBD-R33 fusions, demonstrating the importance of α5 in the interaction of N-WASP with $EspF_U$. Truncations from R33 to R30 or R27 decrease stability by ~2 kcal/mol. Thus, residues beyond Ala30 contribute thermodynamically to GBD-R33 interaction, despite the absence of discrete structure in these regions. Similar contributions to affinity through disordered regions have been observed in other systems as well[24]. Truncation of all (R14) or part (R18) of the $EspF_U$ C-terminal arm decreases the stability further, indicating that the arm contributes significantly to binding of the GBD to $EspF_U$. These unfolding studies mirror direct binding measurements. R33 and R18 bind N-WASPC with K_D values of 35 and 4000 nM, respectively (Fig. 1D), corresponding to a difference in free energy of 2.9 kcal/mol. This value agrees closely with the stability difference between the two GBD-fusions (2.6 kcal/mol, Fig. 1D). Finally, these differences in binding correspond well to the activities of the $EspF_U$ mutants in N-WASP mediated actin assembly assays, where activity decreases in concert with strength of interaction (Figs. 1B, D).

To test how the biophysical properties of $EspF_U$-N-WASP interaction relate to biological function, we examined the ability of $EspF_U$ derivatives to induce localized actin assembly in mammalian cells. To uncouple Tir-mediated recruitment of $EspF_U$ from $EspF_U$ function in pedestal generation after recruitment, we replaced the C-terminal cytoplasmic domain of Tir with two repeats of $EspF_U$ (giving $Tir\Delta C\text{-}R_2$). We expressed $Tir\Delta C\text{-}R_2$ in mouse fibroblast-like cells, where it inserted into the plasma membrane, and then clustered it by adding *E. coli* expressing intimin. Immunostaining revealed foci of clustered Tir and N-WASP coincident with bound bacteria (Fig. 3A). Similarly, F-actin strongly colocalized with Tir. In contrast, a control Tir derivative (TirΔC) lacking cytoplasmic elements did not recruit N-WASP or produce actin pedestals (Fig. 3). Mutation of Leu12 to Ala in both $EspF_U$ repeats (giving $Tir\Delta C\text{-}R_2{}^{VL*}$) also abolished both actin assembly and N-WASP recruitment (Fig. 3A), consistent with the decreased binding of this mutant to N-WASP *in vitro* (Fig. 1). To examine the activity of $EspF_U$ truncation mutants, we modified this assay to analyze derivatives of one $EspF_U$ repeat unit. As predicted by *in vitro* data (Fig. 1), the triple V4A/L8A/L12A mutant, TirΔCR47***, was also unable to assemble actin (Fig. S12). Truncation of R47 to R33 decreased activity, likely due to the loss of most of the proline-rich region, which in EspF is known to bind SH3-containing proteins to promote actin assembly[23] (Fig. 3B). R30 and R27 showed even lower actin assembly levels, consistent with the diminished $N\text{-}WASP_C$ binding by these proteins compared to R33 (Fig. 1). Finally, R14, which bound $N\text{-}WASP_C$ only very weakly (Fig. 1), did not promote actin assembly above background levels. Together, these data show that the ability of $EspF_U$ derivatives to promote actin assembly *in vivo* reflects the physical interactions between $EspF_U$ and WASP *in vitro*.

The GBD-R33 and GBD-C complexes are remarkably similar (Fig. 2). In both cases, ligand binding causes the GBD to fold into a β-hairpin and four helices. The backbone r. m. s. d. between the average GBD coordinates in the two structures is only 0.95 Å (residues 247–310). This structural similarity is reflected in high chemical shift similarity: the average GBD

chemical-shift differences are 0.015 ppm for HN, 0.062 ppm for H^{α}, 0.043 ppm for H^{β}, 0.21 ppm for C^{α}, and 0.30 ppm for C^{β}. The most significant chemical shift differences between the two complexes occur in α2, which contacts the extended arm of $EspF_U$ in the GBD-R33 complex, but is solvent exposed in the GBD-C complex. The WASP C helix and $EspF_U$ helix bind the same site on the GBD in the same orientation through analogous hydrophobic contacts involving similar sequences (Fig. 1A, Fig. S9). $EspF_U$ makes additional contacts to the GBD through its C-terminal arm, which are not seen in the bound C region helix in autoinhibited WASP. These contacts contribute to the much higher WASP affinity of $EspF_U$ compared to its eukaryotic counterparts[21]. The combined structural and biochemical data lead to a clear and simple mechanism for WASP/N-WASP activation by a single repeat element of $EspF_U$: displacement of the VCA through competitive binding to a common site on the folded GBD.

We have described the autoinhibited GBD-VCA structure as composed of three layers, analogous to the three layers of the GBD-R33 structure, with the C region of the VCA substituting for R33[7]. Three structurally distinct mechanisms for relieving autoinhibition of WASP/N-WASP are now known that involve attacks on distinct regions of this fold (Fig. S13). Cdc42 globally destabilizes the GBD by binding to the first layer of structure. Similarly, following phosphorylation of the conserved Tyr291/256 in WASP/N-WASP, SH2 domains can also destabilize the GBD by binding to this site in the second layer. EHEC have evolved the simplest and structurally most direct means of releasing the VCA: $EspF_U$ binds to the GBD-VCA interface, displacing the VCA from the folded GBD by structural competition. Of the three known allosteric mechanisms, only this latter one is akin to those found in most other autoinhibited multi-domain systems, where activation is driven by rearrangements of intact functional modules. The diversity of WASP regulation likely originates from the intrinsically unstructured nature of the GBD, which enables its broad binding specificity. Since the folded GBD is structurally incompatible with Cdc42/SH2 binding, $EspF_U$ can displace the VCA while simultaneously preventing interactions with eukaryotic activators, thus sequestering WASP proteins away from their normal signaling pathways. This, coupled with very high affinity binding, allows EHEC to subvert the host actin cytoskeleton to its own ends.

Methods Summary

Protein Expression and Purification

$EspF_U$ and WASP proteins were expressed in bacteria as either His_6- or GST-fusions, and purified by affinity and conventional chromatographies. Bovine Arp2/3 complex and rabbit skeletal muscle actin were purified as described[25, 26].

Biochemical Assays

All biochemical assays were performed in KMEI buffer (10 mM imidazole pH 7.0, 50 mM KCl, 1 mM $MgCl_2$, and 1 mM EGTA), or KMEI plus 5 mM β-mercaptoethanol at 25 °C. *Actin Assembly*. Actin assembly assays were performed as described[25], with 4 μM actin (5% pyrene labeled) and 10 nM Arp2/3 complex. Filament barbed end concentrations were calculated as described[27]. *Chemical Denaturation*. GBD-$EspF_U$ fusion proteins (10 μM) were denatured with guanidine hydrochloride. Tryptophan fluorescence emission (λ_{ex} = 295 nm, λ_{em} = 320 nm, 355 nm) was fit to a six parameter equation28 to yield $\Delta G_{unfolding}$. *Isothermal Titration Calorimetry*. $EspF_U$ proteins were titrated into N-$WASP_C$ in a Microcal VP-ITC microcalorimeter. Baseline was corrected for $EspF_U$ addition to buffer. Data were fit to a single site binding model.

Mammalian Cell Culture

Mouse fibroblast-like cells were transfected with HA-Tir-$EspF_U$ fusions as described[1]. Transfected cells were treated with *E. coli* expressing intimin for 3.5 hours (for Tir-R_2 fusions)

or antibodies recognizing the extracellular domain of EHEC Tir (gift from A. Donohue-Rolfe, Tufts University School of Veterinary Medicine), followed by *S. aureus* particles (Pansorbin; Calbiochem) (for Tir fusions with a single $EspF_U$ repeat).

Immunofluorescence Microscopy

Monolayers were fixed and permeabilized as described[29]. Cells were treated with HA.11 or α-N-WASP (gift from S. Snapper), washed and treated with Alexa488 goat anti-mouse antibody (1:200; Molecular Probes) or Alexa568 goat anti-rabbit antibody (1:150; Molecular Probes) respectively. F-actin was stained with Alexa568-phalloidin (1:100; Molecular Probes).

NMR Spectroscopy and Structure Calculation

The structure of the complex of GBD (residues 242–310) and R33 (residues 1–33 in Fig. 1, corresponding to residues 268–300 in $EspF_U$ (Fig. S1)) was determined in iterative fashion based on NOE, dihedral and hydrogen bond restraints using ARIA 2.1[30].

Additional Methods

Protein Expression and Purification

To simplify nomenclature, $EspF_U$ residues are numbered 1–47 below and throughout the text (cf. Fig. 1), corresponding to residues 268–314 of the full length protein (Fig. S1). WASP GBD (residues 242–310), $EspF_U$ R33 (residues 1–33), R33 mutants, GBD-R33 (WASP 242-310 -GGSGGSHM- $EspF_U$ 1-33) and other GBD-repeat fusions were cloned into a modified pGEX-2T vector with a Tev protease cleavage site at the C-terminus of GST. $EspF_U$ R_5 (residues 80–314) was cloned into a pET15b vector. $EspF_U$ R47 (residues 1–47) was cloned into a modified pET19b vector with a His_{10}-ubiquitin-Tev protease site at the N-terminus. All proteins were expressed in *E. coli* strain BL21(DE3). Uniform $^{15}N/^{13}C$ labeling of proteins was carried out in M9 minimum media supplemented with $^{15}NH_4Cl$ and ^{13}C-gluose as the sole nitrogen and carbon sources. Samples of U-[^{15}N,^{2}H], Ile-[$^{13}C^{\delta}H_3$], Leu-[$^{13}CH_3$,$^{12}CD_3$], Val-[$^{13}CH_3$,$^{12}CD_3$]) labeled proteins were obtained from bacterial growth in M9 D_2O media containing 3 g/l of U-[^{2}H]-glucose, 1 g/l of $^{15}NH_4Cl$, and 50 mg/l of 2-keto-3-methyl-d_3-3-d_1-4-^{13}C-butyrate and 50 mg/l 4-[^{13}C,^{1}H]-3,3-^{2}H-α-ketobutyrate (the latter two, added 1 hr before induction)[31]. The 3,3-[^{1}H] or the 3-[^{1}H] positions of commercially available α-ketobutyrate or 2-keto-3-methyl-butyrate were exchanged to ^{2}H prior to use, according to the procedure of Gardner et al.[32]. $EspF_U$ R14 and R18 peptides were synthesized at the UT Southwestern Protein Chemistry Technology Center and quantified by amino acid analysis.

Cells expressing GBD and GBD-$EspF_U$ fusions were lysed by sonication in GST buffer (20 mM Tris pH 8.0, 100 mM NaCl, 1 mM DTT, and 1 mM EDTA) with protease inhibitors. Cleared lysates were applied to glutathione sepharose 4B (GE Healthcare). Following wash, GST-tagged proteins were eluted in GST buffer containing 10 mM reduced glutathione. Proteins were concentrated, cleaved with Tev protease to separate the GST tag, diluted three-fold into QA buffer (20 mM Tris pH 8.0, 1 mM DTT, and 1 mM EDTA) and loaded onto an anion exchange column (Mono Q, GE Healthcare) equilibrated in QA buffer. The column was developed with a linear gradient from 0% to 50% QB buffer (Buffer A plus 1 M NaCl) in 10 bed volumes. Protein-containing fractions were further purified by size exclusion chromatography (Superdex 75 column, GE Healthcare). GST-GBD was purified similarly, except that the Tev protease cleavage was omitted. $EspF_U$ R33 and its mutants were purified similarly, except that in the anion-exchange step the protein was collected in the flow through. His_{10}-ubiquitin tagged $EspF_U$ R47 was retained from cleared bacterial lysate on a Ni-NTA column (Qiagen), eluted with an imidazole gradient, desalted into QA buffer and cleaved with Tev protease to remove the His_{10}-ubiquitin tag. Subsequent anion exchange and size exclusion chromatographies were the same as described for $EspF_U$ R33. His_6-$EspF_U$ R_5 was purified by

Ni affinity chromatography and buffer exchanged into SA buffer (50 mM sodium phosphate pH 6.0, 1 mM DTT, and 1 mM EDTA). Thrombin (GE Healthcare) cleaved $EspF_U$ R_5 was purified by cation exchange (Mono S, GE Healthcare) in a gradient from 300 mM to 600 mM NaCl over 10 column volumes. Fractions containing $EspF_U$ R_5 were pooled and further purified by gel filtration chromatography (Superdex 200, GE Healthcare). WASP GBD-VCA, N-$WASP_C$ (residues 193–501), bovine Arp2/3 complex and rabbit skeletal muscle actin were purified as described previously[25–27].

Pull-Down Assays

GST-GBD was immobilized on Glutathione-sepharose 4B beads (~75 nmole/ml beads, GE Healthcare). Beads (60 µl) were incubated with 30 µM $EspF_U$ R33 and 15 µM WASP VCA separately in a final volume of 230 µl and washed three times. The same volume of beads containing VCA-bound GST-GBD was further incubated with 200 µM R33 and washed four times. Flow through and beads were analyzed by SDS-PAGE stained with Coomassie Blue.

Mammalian Cell Culture and Immunofluorescence Microscopy

To create transfection plasmids expressing Tir-$EspF_U$ fusions (all N-terminally HA-tagged), DNA fragments encoding $EspF_U$ R14, R30, R33, R47, R_2 (repeats 4–5) and point mutants were cloned into the KpnI and BamHI sites of pHN-TirΔC[1]. Mouse fibroblast-like cells were cultured in six-well plates in DMEM plus 10% FBS and transfected with 1 µg of plasmid per well for 12–16 h using Lipofectamine Plus reagent (Invitrogen)[1]. Cells were reseeded onto 12-mm glass coverslips to achieve 50–75% confluency after an additional 24 h of growth. Transfected cells expressing TirΔC-R_2 proteins were treated with an *E. coli* expressing intimin for 3.5 hours. Cells expressing TirΔC fused to a single $EspF_U$ repeat were treated with a 1:200 dilution of antibodies raised against the extracellular domain of EHEC Tir (anti-TirM) for 30 min, washed to remove excess antibody, and then treated with *S. aureus* particles (Pansorbin; Calbiochem) for a further 2.5 h. In all cases, monolayers were fixed in PBS+4% paraformaldehyde for 30 minutes and permeabilized with 0.1% Triton-X-100 as described[29]. Cells were then treated with HA.11 (diluted 1:500 in PBS+1%BSA) or HA.11 and α-N-WASP (1:500) for 30 minutes prior to washing and addition of Alexa488 goat anti-mouse antibody (1:200; Molecular Probes) or Alexa568 goat anti-rabbit antibody (1:150). F-actin was identified by staining with Alexa568-phalloidin (1:100; Molecular Probes).

NMR Spectroscopy and Structure Calculation

The complex between GBD and R33 was isolated by gel filtration chromatography (in 50 mM sodium phosphate pH 6.8, 100 mM NaCl, 1 mM DTT, and 1 mM EDTA), and concentrated to 1-1.5 mM for all NMR experiments. Backbone and sidechain chemical shift assignments were obtained using standard triple-resonance methods in $^{15}N/^{13}C$-labeled samples [33, 34]. A total of 1552 distance restraints were obtained from 2D ^1H-NOESY, 3D ^{15}N-edited NOESY (τ_{mix} = 100 ms), and 4D $^{13}C/^{13}C$-edited NOESY (τ_{mix} = 75 ms)[35] spectra. One hundred intermolecular NOEs were identified in a ^{13}C-filtered NOESY spectrum (τ_{mix} = 100 ms) of $^{13}C,^{15}N$-GBD in complex with unlabeled R33 recorded in D_2O[36]. A total of 165 unambiguously assigned NOEs define the GBD-R33 interface. Backbone dihedral angles were restrained based on chemical shift analyses in the program TALOS[37] (maximum of 30° or the standard deviation observed in the TALOS database matches). Hydrogen bond restraints (HN-O distance, 1.5-2.8 Å; N-O distance, 2.4 – 3.5 Å) were applied to amide groups that were protected for > 1 hour in a sample of a ^{15}N-GBD-R33 fusion protein freshly dissolved in D_2O NMR buffer. Structures were calculated and iteratively refined using the program ARIA 2.1[30]. Intermolecular NOEs were assigned manually, in iterative fashion, from the ^{13}C-filtered NOESY spectrum, and assigned distance restraints within ARIA 2.1. Other NOEs were assigned automatically within ARIA 2.1. In the final iteration, structures were refined in

explicit water to improve sidechain packing and hydrogen bonding[38]. All spectra were processed and analyzed using NMRPipe[39] and NMRView[40]. The twenty final lowest energy conformers were analyzed with ProCheckNMR[41]. Structure figures were generated with Ribbons[42] and PyMOL[43].

Supplementary Material

Refer to Web version on PubMed Central for supplementary material.

Acknowledgements

We thank Dr. Takanori Otomo for discussion and assistance on biochemical assays and NMR spectroscopy; Pilong Li, Ilidio Martins and Drs. Carlos A. Amezcua, Kevin H. Gardner, and Qiong Wu for assistance with NMR spectroscopy and structure calculations; Drs. Gaya K. Amarasinghe and Daisy W. Leung for sharing reagents; Derek Trobaugh, Jason Rennie and Douglas Robbins for technical assistance; Dr. Shae B. Padrick for help with Mathematica, and Drs. Xiaolan Yao and S.B.P. for assistance in writing and for critical reading of the manuscript. This work was supported by grants from the NIH (NIH-R01-GM56322 to M.K.R.; NIH-R01-AI46454 to J.L.), and Welch Foundation (I–1544 to M.K.R.), and a Chilton Foundation Fellowship to H.-C. C.

References

1. Campellone KG, Robbins D, Leong JM. EspFU is a translocated EHEC effector that interacts with Tir and N-WASP and promotes Nck-independent actin assembly. Dev Cell 2004;7:217–228. [PubMed: 15296718]
2. Garmendia J, et al. TccP is an enterohaemorrhagic Escherichia coli O157:H7 type III effector protein that couples Tir to the actin-cytoskeleton. Cell Microbiol 2004;6:1167–1183. [PubMed: 15527496]
3. Campellone KG, et al. Enterohaemorrhagic Escherichia coli Tir requires a C-terminal 12-residue peptide to initiate EspFu-mediated actin assembly and harbours N-terminal sequences that influence pedestal length. Cell Microbiol 2006;8:1488–1503. [PubMed: 16922867]
4. Garmendia J, Carlier MF, Egile C, Didry D, Frankel G. Characterization of TccP-mediated N-WASP activation during enterohaemorrhagic Escherichia coli infection. Cell Microbiol 2006;8:1444–1455. [PubMed: 16922863]
5. Lommel S, Benesch S, Rohde M, Wehland J, Rottner K. Enterohaemorrhagic and enteropathogenic Escherichia coli use different mechanisms for actin pedestal formation that converge on N-WASP. Cell Microbiol 2004;6:243–254. [PubMed: 14764108]
6. Buck M, Xu W, Rosen MK. A two-state allosteric model for autoinhibition rationalizes WASP signal integration and targeting. J Mol Biol 2004;338:271–285. [PubMed: 15066431]
7. Kim AS, Kakalis LT, Abdul-Manan N, Liu GA, Rosen MK. Autoinhibition and activation mechanisms of the Wiskott-Aldrich syndrome protein. Nature 2000;404:151–158. [PubMed: 10724160]
8. Torres E, Rosen MK. Contingent phosphorylation/dephosphorylation provides a mechanism of molecular memory in WASP. Mol Cell 2003;11:1215–1227. [PubMed: 12769846]
9. Munter S, Way M, Frischknecht F. Signaling during pathogen infection. Sci STKE 2006;2006:re5. [PubMed: 16705131]
10. Caron E, et al. Subversion of actin dynamics by EPEC and EHEC. Curr Opin Microbiol 2006;9:40–45. [PubMed: 16406772]
11. Hayward RD, Leong JM, Koronakis V, Campellone KG. Exploiting pathogenic Escherichia coli to model transmembrane receptor signalling. Nat Rev Microbiol 2006;4:358–370. [PubMed: 16582930]
12. Gruenheid S, Finlay BB. Microbial pathogenesis and cytoskeletal function. Nature 2003;422:775–781. [PubMed: 12700772]
13. Galan JE, Cossart P. Host-pathogen interactions: a diversity of themes, a variety of molecular machines. Curr Opin Microbiol 2005;8:1–3. [PubMed: 15694849]
14. Rangel JM, Sparling PH, Crowe C, Griffin PM, Swerdlow DL. Epidemiology of Escherichia coli O157:H7 outbreaks, United States, 1982–2002. Emerg Infect Dis 2005;11:603–609. [PubMed: 15829201]

15. DeVinney R, et al. Enterohemorrhagic Escherichia coli O157:H7 produces Tir, which is translocated to the host cell membrane but is not tyrosine phosphorylated. Infect Immun 1999;67:2389–2398. [PubMed: 10225900]
16. Higgs HN, Pollard TD. Regulation of actin filament network formation through Arp2/3 complex: Activation by a diverse array of proteins. Ann. Rev. Biochem 2001;70:649–676. [PubMed: 11395419]
17. Kelly AE, Kranitz H, Dotsch V, Mullins RD. Actin binding to the central domain of WASP/Scar proteins plays a critical role in the activation of the Arp2/3 complex. J Biol Chem 2006;281:10589–10597. [PubMed: 16403731]
18. Panchal SC, Kaiser DA, Torres E, Pollard TD, Rosen MK. A conserved amphipathic helix in WASP/Scar proteins is essential for activation of Arp2/3 complex. Nat Struct Biol 2003;10:591–598. [PubMed: 12872157]
19. Rohatgi R, et al. The interaction between N-WASP and the Arp2/3 complex links Cdc42-dependent signals to actin assembly. Cell 1999;97:221–231. [PubMed: 10219243]
20. Buck M, Xu W, Rosen MK. Global disruption of the WASP autoinhibited structure on Cdc42 binding. Ligand displacement as a novel method for monitoring amide hydrogen exchange. Biochemistry 2001;40:14115–14122. [PubMed: 11714264]
21. Leung DW, Rosen MK. The nucleotide switch in Cdc42 modulates coupling between the GTPase-binding and allosteric equilibria of Wiskott-Aldrich syndrome protein. Proc Natl Acad Sci U S A 2005;102:5685–5690. [PubMed: 15821030]
22. Garmendia J, et al. Distribution of tccP in clinical enterohemorrhagic and enteropathogenic Escherichia coli isolates. J Clin Microbiol 2005;43:5715–5720. [PubMed: 16272509]
23. Alto NM, et al. The type III effector EspF coordinates membrane trafficking by the spatiotemporal activation of two eukaryotic signaling pathways. J Cell Biol 2007;178:1265–1278. [PubMed: 17893247]
24. Volkman BF, Prehoda KE, Scott JA, Peterson FC, Lim WA. Structure of the N-WASP EVH1 domain-WIP complex: insight into the molecular basis of Wiskott-Aldrich Syndrome. Cell 2002;111:565–576. [PubMed: 12437929]
25. Higgs HN, Blanchoin L, Pollard TD. Influence of the C terminus of Wiskott-Aldrich syndrome protein (WASp) and the Arp2/3 complex on actin polymerization. Biochemistry 1999;38:15212–15222. [PubMed: 10563804]
26. Cooper JA, Pollard TD. Methods to measure actin polymerization. Methods Enzymol 1982;85(Pt B): 182–210. [PubMed: 6889668]
27. Leung DW, Morgan DM, Rosen MK. Biochemical properties and inhibitors of (N-)WASP. Methods Enzymol 2006;406:281–296. [PubMed: 16472665]
28. Pace CN. Measuring and increasing protein stability. Trends Biotechnol 1990;8:93–98. [PubMed: 1367432]
29. Campellone KG, Giese A, Tipper DJ, Leong JM. A tyrosine-phosphorylated 12-amino-acid sequence of enteropathogenic Escherichia coli Tir binds the host adaptor protein Nck and is required for Nck localization to actin pedestals. Mol Microbiol 2002;43:1227–1241. [PubMed: 11918809]
30. Rieping W, et al. ARIA2: automated NOE assignment and data integration in NMR structure calculation. Bioinformatics 2007;23:381–382. [PubMed: 17121777]
31. Goto NK, Gardner KH, Mueller GA, Willis RC, Kay LE. A robust and cost-effective method for the production of Val, Leu, Ile (delta 1) methylprotonated 15N-, 13C-, 2H-labeled proteins. J Biomol NMR 1999;13:369–374. [PubMed: 10383198]
32. Gardner KH, Kay LE. Production and Incorporation of 15N, 13C, 2H (1Hd1 Methyl) Isoleucine into Proteins for Multidimensional NMR Studies. J. Am. Chem. Soc 1997;119:7599–7600.
33. Clore GM, Gronenborn AM. Multidimensional heteronuclear nuclear magnetic resonance of proteins. Methods Enzymol 1994;239:349–363. [PubMed: 7830590]
34. Muhandiram DR, Kay LE. Gradient-enhanced triple-resonance three-dimensional NMR experiments with improved sensitivity. J. Magn. Reson. Ser. B 1994;103
35. Clore GM, Kay LE, Bax A, Gronenborn AM. Four-dimensional 13C/13C-edited nuclear Overhauser enhancement spectroscopy of a protein in solution: application to interleukin 1 beta. Biochemistry 1991;30:12–18. [PubMed: 1988012]

36. Zwahlen C, et al. Methods for Measurement of Intermolecular NOEs by Multinuclear NMR Spectroscopy: Application to a Bacteriophage Lamda N-Peptide/ boxB RNA Complex. J. Am. Chem. Soc 1997;119:6711–6721.

37. Cornilescu G, Delaglio F, Bax A. Protein backbone angle restraints from searching a database for chemical shift and sequence homology. J Biomol NMR 1999;13:289–302. [PubMed: 10212987]

38. Linge JP, Williams MA, Spronk CA, Bonvin AM, Nilges M. Refinement of protein structures in explicit solvent. Proteins 2003;50:496–506. [PubMed: 12557191]

39. Delaglio F, et al. NMRPipe: a multidimensional spectral processing system based on UNIX pipes. J Biomol NMR 1995;6:277–293. [PubMed: 8520220]

40. Johnson BA, Blevins RA. NMR View: A computer program for the visualization and analysis of NMR data. J Biomol NMR 1994;4:603–614.

41. Laskowski RA, Rullmannn JA, MacArthur MW, Kaptein R, Thornton JM. AQUA and PROCHECK-NMR: programs for checking the quality of protein structures solved by NMR. J. Biomol. NMR 1996;8:477–486. [PubMed: 9008363]

42. Carson, M.; Charles, WC., Jr.; Robert, MS. Methods in Enzymology. Academic Press; 1997. p. 493-502.

43. DeLano, WL. The PyMOL User's Manual. San Carlos, CA, USA: DeLano Scientific; 2002.

44. Cantor, CR.; Schimmel, PR. Biophysical Chemistry, Part III: The Behavior of Biological Macromolecules. New York: W. H. Freeman and Company; 1980.

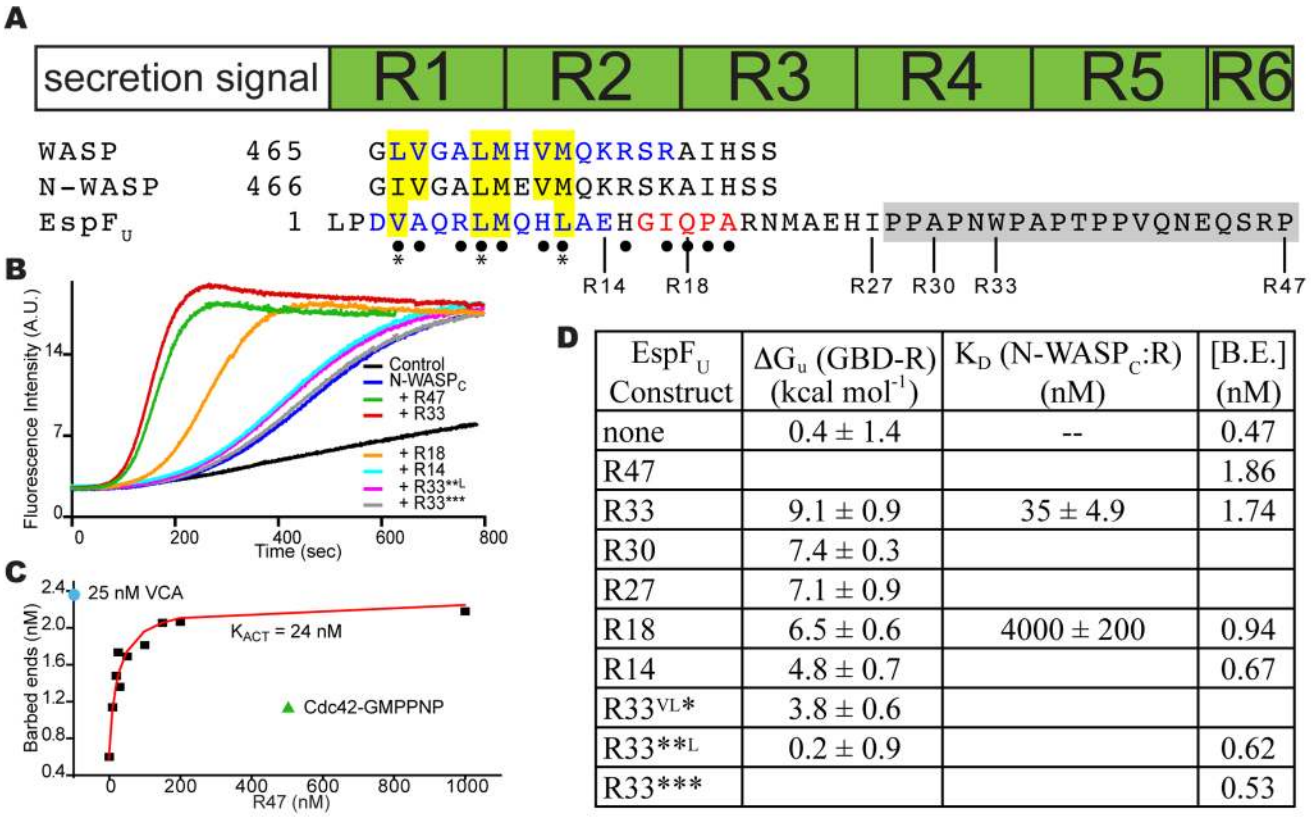

D

EspF$_U$ Construct	ΔG_u (GBD-R) (kcal mol^{-1})	K_D (N-WASP$_C$:R) (nM)	[B.E.] (nM)
none	0.4 ± 1.4	--	0.47
R47			1.86
R33	9.1 ± 0.9	35 ± 4.9	1.74
R30	7.4 ± 0.3		
R27	7.1 ± 0.9		
R18	6.5 ± 0.6	4000 ± 200	0.94
R14	4.8 ± 0.7		0.67
R33^{VL}*	3.8 ± 0.6		
R33**^{L}	0.2 ± 0.9		0.62
R33***			0.53

Figure 1. A single repeat of EspF$_U$ activates WASP/N-WASP with high potency

A. Sequence alignment of WASP and N-WASP VCA C regions and the fifth repeat element of EspF$_U$. Helix residues in the autoinhibited GBD-C structure and GBD-R33 complex are blue. Residues in the extended EspF$_U$ arm are red. Aligned hydrophobic residues are boxed in yellow. EspF$_U$ residues that contact the GBD are indicated by •. Sites of EspF$_U$ mutations used in panels B and D are indicated by *. Proline-rich motif is boxed in gray. The C-termini of EspF$_U$ single repeat constructs used throughout this work are indicated below the sequence. **B.** Pyrene-actin fluorescence measured during assembly of 4 μM actin (5% pyrene-labeled) plus 10 nM Arp2/3 complex (black) plus 25 nM N-WASP$_C$ (blue) plus 500 nM of: R47 (green), R33 (red), R18 (orange), R14 (cyan), R33**^{L} (pink) or R33*** (V4A/L8A/L12A, grey). **C.** Concentration of filament barbed ends produced during assembly of 4 μM actin by 10 nM Arp2/3 complex, 25 nM N-WASP$_C$ and increasing concentrations of R47 (black squares; red curve shows fit to single site binding isotherm) or 500 nM Cdc42-GMPPNP (green triangle). Blue circle shows barbed ends produced by actin plus Arp2/3 plus 25 nM N-WASP VCA. **D.** For EspF$_U$ proteins listed, table shows free energy of unfolding of GBD-EspF$_U$ fusion, dissociation constant for binding to N-WASP$_C$, and actin filament barbed ends produced by assays in panel B. In "none" row, ΔGu represents melting of the isolated GBD, B.E. represents assays performed with only N-WASP$_C$ and Arp2/3 complex.

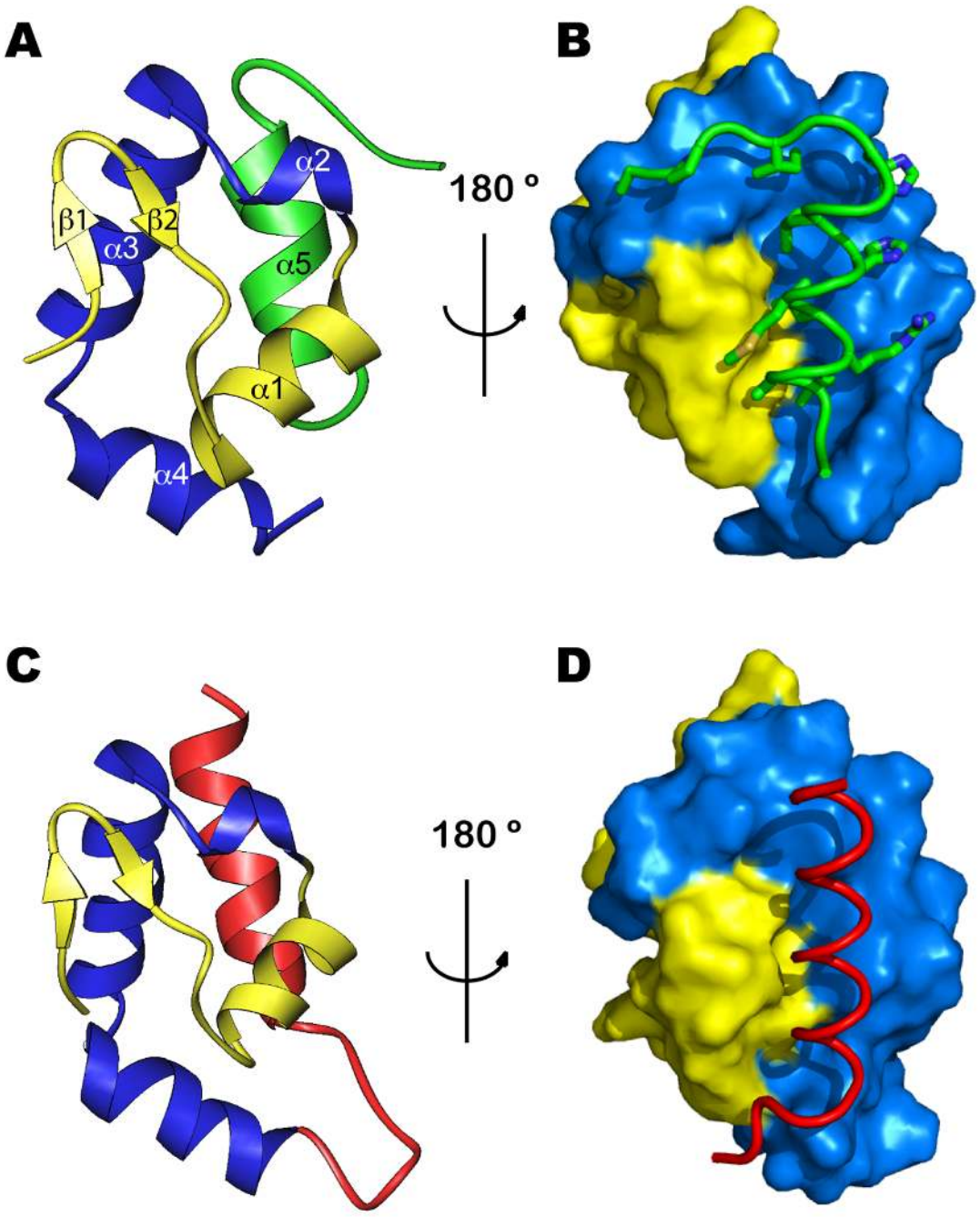

Figure 2. Structures of the WASP GBD in complex with different ligands

A, B. Complex of WASP GBD and EspFU R33. Structure is colored: layer 1 (WASP 250–276), yellow; layer 2 (WASP 277–310), blue; layer 3 ($EspF_U$ 2–20), green. In B, GBD is shown as surface representation, R33 is shown as a ribbon with sticks for sidechains that contact the GBD. Views are related by 180° rotation about a vertical axis. **C, D.** Autoinhibited WASP (GBD-C^7). GBD colored as in A; C region of WASP VCA is red. Representation and views are as in panels A and B.

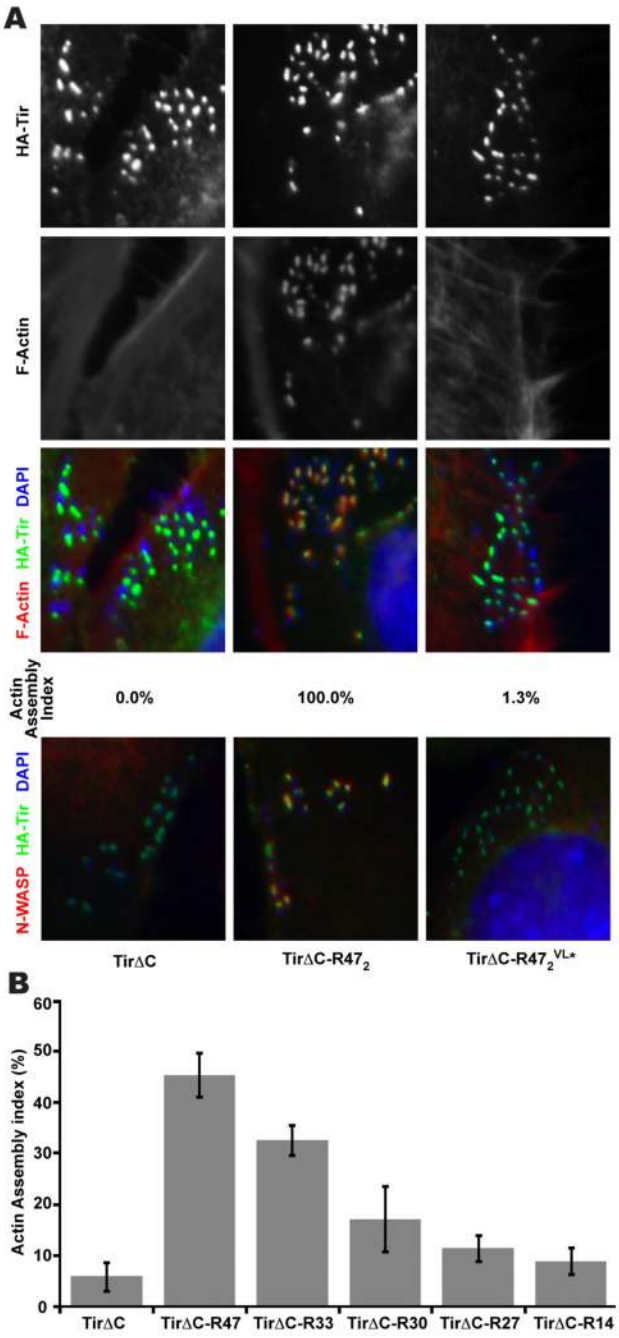

Figure 3. EspF$_U$ induces actin pedestal formation

A. Cells expressing the TirΔC, TirΔC-R$_2$ or TirΔC-R$_2$ ^{VL*} (with N-terminal HA-tags) were challenged with *E. coli* expressing intimin, and stained with anti-HA antibody (green) and Alexa568-phalloidin (red, left panels) or anti-N-WASP antibody (red, right panels). Colocalization is yellow in merged images. The % of transfected cells harboring at least five F-actin foci was quantified (Actin Assembly Index). Bacteria were visualized by DAPI staining. **B.** Cells expressing Tir-repeat proteins were challenged with anti-Tir antibody and *S. aureus* particles and Actin Assembly Index was determined. In A and B data represent mean +/− SD from at least two samples with 20-50 cells examined per sample.